LA-UR -92-1271

Conf

LA-UR--92-1271

DE92 013537

Los Alamos National Laboratory is operated by the University of California for the United States Department of Energy under contract W-7405-ENG-36

TITLE A MODEL FOR THE INTERFACIAL SHEAR IN VERTICAL, ADIABATIC, ANNULAR-MIST FLOW

AUTHOR(S) M. W. Cappiello

SUBMITTED TO 1992 National Heat Transfer Conference
August 9-12, 1992
San Diego, CA

Los Alamos Los Alamos National Laboratory
Los Alamos, New Mexico 87545

A MODEL FOR THE INTERFACIAL SHEAR IN VERTICAL, ADIABATIC, ANNULAR-MIST FLOW

M. W. Cappiello
Los Alamos National Laboratory
Reactor Design and Analysis Group
Los Alamos, NM 87545
665-1558

ABSTRACT

A model is developed for the interfacial shear in upward, vertical, adiabatic, annular-mist flow. The model accounts for the momentum of both the droplet and film components and is applicable to the two-fluid approximation. Three computer programs are developed to evaluate the sensitivity of the droplet drag coefficient on the droplet velocity calculation, to solve the two-fluid set of equations by iteration, and to evaluate the required film friction factor from the data. The results of the sensitivity calculation show that a constant drag coefficient of 0.44 for the droplet is sufficient for estimating the droplet velocity over a typical range of gas velocities. Several film friction factor correlations from the literature were tested against the existing data of Hossfeld and Barathan. It was found that a modified effective roughness correlation proposed by Wallis performs the best overall in predicting the data for both small- and large-diameter pipes. The Electrical Power Research Institute drift-flux correlation and the Barathan correlation consistently underpredict the data. The use of the Henstock and Hanratty correlation predicts an incorrect trend. A new correlation is developed that better predicts the data over the entire range of gas injection rates.

NOMENCLATURE

Variable	Description
V	Velocity (m/s)
F	Force (N)
A	Area (m^2)
Mid	Force per unit volume (N/m^3)
C_d	Form drag coefficient
Ci	Interfacial drag coefficient (kg/m^4)
Vol	Volume (m^3)
D	Diameter (m)
P	Pressure (N/m^2)
g_c	Gravitational acceleration (m/s^2)
J	Superficial velocity (m/s)
f	Friction factor
E	Entrainment fraction
W	Weber number
Re	Reynolds Number
ρ	Density (kg/m^3)
μ	Viscosity ($N\text{-}s/m^2$)
σ	Surface tension (N/m)
Γ	Phase change ($kg/s\text{-}m^3$)
α	Area or volume fraction
τ	Shear stress (N/m^2)

Subscripts

k	phase or component
l	liquid
d	droplet
f	film
g	gas
i	interface
p	projected
c	core
w	wall
e	entrained

INTRODUCTION

Computer codes are often used for the analysis of Light Water Reactor (LWR) abnormal and operational transients. Because the transients involve rapid depressurizations and boiling, the codes must be able to predict the thermal-hydraulic phenomena involved in two-phase flow. Many approaches have been taken to this problem. One of the most successful is the non-equilibrium two-fluid approach such as that used in the Transient Reactor Analysis Code (TRAC).[1] Here, a mass, momentum, and energy equation is solved for each phase in a Eulerian mesh scheme that represents the reactor primary system. For this approach, the system of equations is brought to closure through the equations of state and interfacial constitutive relations for the exchange of mass, momentum, and energy. The interfacial constitutive relation in the momentum equations is often referred to as the interfacial shear. It is of considerable importance to accurately calculate this term because it can often dominate the momentum equations and directly affect the relative movement and mass fractions of the phases.

Typical flow regimes observed in vertical two phase flow are bubbly, bubbly slug, churn, annular, and annular

mist. The annular-mist flow regime occurs at high gas fluxes that can occur during postulated large-break loss-of-coolant accidents (LBLOCAs) in pressurized water reactors (PWRs) and is often encountered in the oil and gas industry during oil reprocessing, and in the transport of natural gas. The flow is characterized by gas flowing in the center of the channel, an annular film flowing along the wall, and entrained droplets flowing in the gas core (Fig. 1). The annular film to gas interface is quite agitated, making it similar to a "roughened" surface that might occur in single-phase pipe flow. The droplets are of a variety of sizes and shapes so that a multitude of droplet velocities can be present within the gas core.

To accurately model the mechanisms of annular-mist flow, separate field equations are required for the gas core and liquid film because of the large difference in their respective velocities. In addition, multiple droplet fields are required to model a variety of droplets traveling at different speeds. The use of multiple sets of field equations may be useful in the detailed analysis of separate effects experimental data but can become costly for computation time in system analysis codes. Also, multiple fields are not required for the analysis of other possible flow regimes such as bubbly and churn. Thus, the large, two-phase analysis codes typically employ the two-fluid approximation[1,2] or even less rigorous schemes using homogeneous or drift-flux assumptions. To model annular-mist flow with the two-fluid approximation, one must accept the obvious shortcoming of using a single liquid field to predict the behavior of both the droplets and annular film. However, one can attempt to predict the total liquid flux and liquid fraction with a careful development of the interfacial shear term in the momentum equation. By definition, this term represents the total exchange of momentum between the gas phase the the liquid droplet and film components.

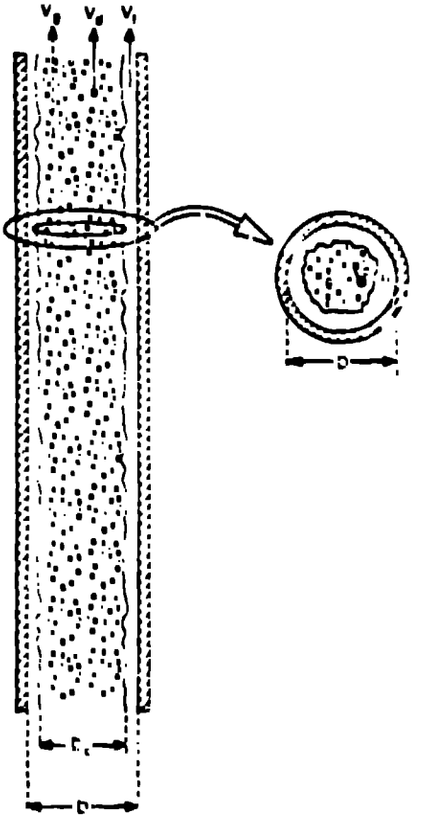

Fig. 1 Representation of annular mist flow

The interfacial shear term that accounts for the momentum of both the droplet and film components is developed below. This model is restricted, however to the case of upward, vertical, adiabatic, annular-mist flow.

Ishii and Chawla [3] formulate the drag laws for dispersed two-phase flow. These models apply to dispersed bubble flow or dispersed droplet flow. In the case of droplets, models are given for the drag coefficient taking into account the effect of droplet distortion from spherical geometry. Comparisons are made to the solid spherical particle drag coefficients and relative velocity data for dispersed flow.

In his book, Wallis (Ref. 4, Chap. 11) presents analysis methods for annular flow. The steady-state two-fluid momentum equation is presented. A correlation for the film interfacial friction is presented based on small-scale (0.0254- to 0.0762-m-diam) pipe data. This correlation is also presented in a modified form to account for the increased density of the gas core resulting from the presence of droplets and the fact that the film at the interface is moving in relation to the mass average film velocity.

Kataoka and Ishii[5] discuss the mechanism for droplet entrainment and provide a correlation for the equilibrium entrainment rate for the case of annular-mist flow. The model is correlated against small-scale data.

Sami[6] develops a three-fluid model for annular-mist flow. Separate conservation equations are written for the vapor, liquid film, and a single droplet field. Entrainment rates, annular film friction, wall friction, and droplet drag are determined using correlations from the literature. The model is assessed against large-diameter annular-mist data (0.125-m diam) and shows good comparisons.

Popov and Rohatgi[7] compare existing correlations for the interfacial shear stress, entrainment inception, and entrainment rate with available flooding data. A steady state two-phase flow model is developed. The formulation consists of a separated flow analysis of the liquid film and a gas droplet mixture. The gas-droplet mixture in the pipe core is treated with the drift flux approximation.

Barathan, Wallis, and Richter[8] correlate the interfacial friction in flooded air–water countercurrent flow as a function of the dimensionless film thickness and pipe size. The model is assessed against data in pipes up to 0.152 m diam.

Henstock and Hanratty[9] develop a correlation for the interfacial friction of the annular film and the film thickness in annular two phase flow. Both horizontal and vertical flow data are used.

Ishii and Mishima[10] develop the detailed two-fluid model for full three-dimensional analysis. The one-dimensional model is developed using area averaging. For annular-mist flow, the Wallis correlation is recommended for the annular film friction factor. Dispersed droplet drag coefficients are given for both solid spherical particles and distorted droplets.

Hossfeld and Barathan[11] present the experimental data for vertical upward annular-mist flow in 0.051- and 0.152-m-diam tubes. Various interfacial friction models are assessed against these data and the data of other experimenters.

Kataoka, Ishii, and Mishima[12] develop a model for the size distribution of droplets in annular two-phase flow. A correlation is recommended for the volume median diameter.

Chexal and Lellouche[13] present a full-range drift-flux correlation for vertical flows. Comparisons are made against a wide range of data including the annular-mist regime. The data include open channel data (up to 0.457 m) and pin bundle geometry. The data considered are "wet wall" where the heat flux from the surface is lower than that required for CHF to occur.

Chexal, Horowitz, and Lellouche[14] provide an assessment of eight void fraction models for vertical flows. Quantitatively, the Chexal-Lellouche model does the best overall. All models perform reasonably well for the conditions for which they were developed.

The review of the literature for annular-mist flow shows that the Wallis correlation, the Henstock and Hanratty correlation, and the Barathan correlation are likely candidates for assessment against the data. In addition, the EPRI drift-flux model is appropriate for testing, although this will be a separate comparison since it cannot be used directly with the two-fluid approximation.

ANNULAR-MIST FLOW

Annular-mist two-phase flow is characterized by a liquid film flowing along the wall and a gas core with entrained droplets (Fig. 1). The surface of the liquid film is highly agitated with droplets being sheared off and entrained into the gas core. Droplets inherently offer more drag and quickly approach the velocity of the gas. Since they also include a tangential component to their velocity, the droplets will eventually strike the film and redeposit. At steady, equilibrium conditions, the entrainment rate and the deposition rates are equal. Correlations (such as Ishii's) exist for the equilibrium entrainment. The droplets can take on a variety of sizes and shapes, thus affecting the drag. The mean diameter of droplets has been correlated by Kataoka,[8] and the effect of the shape on the interfacial drag has been taken into account by Ishii.[4]

For the purpose of this analysis of annular mist flow, the following definitions and relations are given (with reference to Fig. 1).

Subscripts:

- f : annular film
- d : droplets
- g : gas
- l : liquid
- c : core (contains both droplets and gas)

Fluid Velocities:

- V_f : mass average film velocity
- V_d : mass average droplet velocity
- V_g : mass average gas velocity
- V_l : mass average liquid velocity (droplets and film)

Area Fractions:

$$\alpha_f = \frac{A_f}{A}, \text{ film}$$
$$\alpha_d = \frac{A_d}{A}, \text{ droplet} \qquad (1)$$
$$\alpha_g = \frac{A_g}{A}, \text{ gas}$$
$$\alpha_l = \frac{A_l}{A}, \text{ liquid (contains both droplets and film)}$$

where A is the total flow area of the channel and A_k is the area occupied by the field (i.e., drops or film).

Superficial Velocities:

$$j_f = \alpha_f V_f, \text{ film}$$
$$j_d = \alpha_d V_d, \text{ droplet} \qquad (2)$$
$$j_g = \alpha_g V_g, \text{ gas}$$
$$j_l = \alpha_l V_l, \text{ liquid}$$

Equilibrium Entrainment

$$E = \frac{j_d}{j_l}. \qquad (3)$$

Note by this definition that, if the entrainment fraction has a value of 1.0, there can still be a substantial amount of liquid film because the droplet velocity is usually much greater than the liquid film velocity. By the definitions of the area fractions, we have

$$\alpha_f + \alpha_d + \alpha_g = \alpha_l + \alpha_g = 1. \qquad (4)$$

Also, from the definitions of the superficial velocity, a phasic mass flow may be obtained from the multiplication of the superficial velocity times the phasic density times the total area of the channel.

MODEL DEVELOPMENT

Following the development of Ishii,[4] Eq. (5) is given for the conservation of momentum in multiphase flow for the k^{th} phase.

$$\frac{\partial \vec{V}_k}{\partial t} + \vec{V}_k \cdot \nabla \vec{V}_k =$$
$$-\frac{1}{\rho_k}\nabla P \pm \frac{C_i}{\alpha_k \rho_k}\vec{V}_r|\vec{V}_r| - \frac{\Gamma}{\alpha_k \rho_k}\vec{V}_r - \frac{C_{wk}}{\alpha_k \rho_k}\vec{V}_k|\vec{V}_k| + \vec{g} \quad . \qquad (5)$$

The two terms on the left-hand side represent the temporal and spatial acceleration. The first term on the right-hand side is the pressure drop, the second term is the drag at the interface, the third term is the momentum exchange resulting from a change of phase (boiling or condensation), the fourth term is the wall drag, and the last term is the acceleration resulting from gravity. It is noted that the pressure within the phases is assumed to be the same so that no k subscript appears in the pressure drop term. Because we have restricted ourselves to adiabatic, vertical, one-dimensional, co-current, steady flow, the following simplifications are made:

steady $\frac{\partial \vec{V}_k}{\partial t} = 0$

fully developed, incompressible $\nabla \vec{V}_k = 0$

adiabatic, no phase change $\Gamma = 0$

one-dimensional, vertical, co-current $\nabla = \frac{d}{dz}$, $g' = -g_c$, $V'_k = V_k$, $|V'_k| = V_k$

If these terms are combined and multiplied through by the phasic area fraction times the phasic density, the k^{th} phase momentum equation becomes

$$\alpha_k \frac{dP}{dz} = \pm C_i V_r^2 - C_{wk} V_k^2 - \alpha_k \rho_k g_c \quad . \qquad (6)$$

From this equation, the two- and three-fluid approximations to the problem of annular-mist flow are developed.

Two-Fluid Approximation. Substituting l and g subscripts for the liquid and gas phases, respectively, into Eq. (6), we obtain the following relations for the momentum equations

$$\alpha_l \frac{dP}{dz} = C_i V_r^2 - C_{wl} V_l^2 - \alpha_l \rho_l g_c \quad , \qquad (7)$$

and

$$\alpha_g \frac{dP}{dz} = -C_i V_r^2 - C_{wg} V_g^2 - \alpha_g \rho_g g_c \qquad (8)$$

The signs on the interfacial drag term arise because a drag force on the vapor phase provides an equal but opposite pulling force on the liquid phase. It is noted that the absolute values of the relative velocity can be removed because of the assumption of co-current flow and that for the conditions of vertical up flow, $V_g > V_l$.

By using the two-fluid approximation it is inherently assumed that the liquid has only one velocity. In many two-phase flow situations, this is a reasonable assumption. However, it is obvious that for annular-mist flow, the droplets flow at a velocity closer to the vapor velocity and the liquid film velocity is much lower. Therefore, as proposed above, it is necessary to develop an interfacial drag term that can represent the momentum of both the liquid film and droplets. To do this, we first need to consider the three-fluid approximation.

Three-Fluid Approximation. For the three-fluid approximation, the gas field, liquid droplet, and liquid film fields are considered. For the liquid droplets, the momentum equation becomes

$$\alpha_d \frac{dP}{dz} = C_{id}(V_g - V_d)^2 - \alpha_d \rho_l g_c \quad , \qquad (9)$$

where the relative velocity for the interfacial drag term is the difference of the gas and droplet velocities. Also, there is no wall drag term because the droplets do not contact the wall. For the liquid film, the momentum equation becomes

$$\alpha_f \frac{dP}{dz} = C_{if}(V_g - V_f)^2 - C_{wf} V_f^2 - \alpha_f \rho_l g_c \quad , \qquad (10)$$

where the relative velocity for the interfacial drag term is the difference between the gas and liquid film velocities. Here, the film is in contact with the wall, so that the wall drag term is present. We recognize that equations 9 & 10 can be combined and set equal to the liquid momentum equation [Eq. (7)] from the two-fluid approximation because

$$\alpha_l \frac{dP}{dz} = (\alpha_d + \alpha_f)\frac{dP}{dz} \quad . \qquad (11)$$

Therefore, setting the right hand side of Eq. (7) equal to the sum of the liquid droplet and liquid film momentum equations and solving for C_i, the gravitational terms cancel, and we obtain,

$$C_i = \frac{C_{id}(V_g - V_d)^2 + C_{if}(V_g - V_f)^2 + C_{wf}(V_f)^2 - V_f^2)}{V_r^2} \quad . \qquad (12)$$

Thus, the total interfacial drag coefficient, C_i, can be calculated from the individual drag terms for the droplets and the liquid film, plus the difference in the wall drag terms. For a given gas velocity and liquid velocity, C_i can be calculated from the above equation if C_{id}, C_{if}, V_d, and V_f are known. The following sections develop the methods for determining these quantities and bring closure to Eq. (12).

Equilibrium Entrainment

The entrainment fraction is an integral part of the solution for the liquid film and droplet fractions and the film

velocity (which is determined from conservation of mass). Kataoka and Ishii[5] propose a correlation for the equilibrium entrainment in annular-mist two-phase flow. At equilibrium, the entrainment of droplets into the gas core exactly matches the rate of deposition of the droplets from the core onto the liquid film. Thus, the amount of entrainment is defined as in Eq. 4 and varies between 0.0 and 1.0. Kataoka and Ishii correlated several sets of data and provide the following relation.

$$E = \tanh(7.25 \times 10^{-7} We_d^{1.25} Re_l^{0.25}) \quad , \qquad (13)$$

where the liquid Reynolds number is given by

$$Re_l = \frac{\rho_l j_l D}{\mu_l} \quad , \qquad (14)$$

and the droplet Weber number is

$$We_d = \frac{\rho_g j_g^2 D_d}{\sigma} \left(\frac{\Delta\rho}{\rho_g}\right)^{1/3} \quad , \qquad (15)$$

where $\Delta\rho = \rho_l - \rho_g$.

As shown in the correlation, the entrainment varies with the 2.5 power of the gas velocity. Thus, as the gas velocity increases, the entrainment, E, reaches a value of 1.0 quickly.

Droplet Diameter

Kataoka, Ishii, and Mishima[12] propose a correlation for the volume mean diameter of droplets. The mechanism assumed for the generation of the droplets is that of shearing from wave crests such as produced in annular-mist flow. The droplet diameter is given by

$$D_d = \frac{2.0}{\rho_g j_g^2} \left[0.005\, \sigma \left(\frac{\mu_g}{\mu_l}\right)^{2/3} Re_g^{2/3} \left(\frac{\rho_g}{\rho_l}\right)^{1/3}\right] \quad . \qquad (16)$$

Here, the correlation shows an inverse dependence on the gas velocity. Thus, as expected, as the gas velocity increases, the droplet diameter is reduced. The range of data that was used to produce the correlation contained measured diameters from 0.000084 to 0.004 m. In the use of this correlation, the calculated diameter is limited to this range.

Droplet Velocity

The average velocity of the droplets in the upward-moving gas stream can be estimated from a force balance. Assuming steady conditions, the form drag on the droplet is balanced with the force of gravity.

$$C_d \frac{\pi}{4} D_d^2 \rho_g (V_g - V_d)^2 \frac{1}{2} = \Delta\rho g_c \frac{1}{6} \pi D_d^3 \quad . \qquad (17)$$

Solving for V_d.

$$V_d = V_g - \left(\frac{2}{C_d}\right)^{1/2} \left(\frac{\Delta\rho}{\rho_g} g_c \frac{D_d}{2}\right)^{1/2} \quad . \qquad (18)$$

where D_d is the droplet diameter and C_d is the form drag coefficient. Ishii and Chawla[3] recommend a form drag coefficient from the following correlation:

$$C_d = \frac{24}{Re_d} (1.0 + 0.1\, Re_d^{0.75}) \quad , \qquad (19)$$

where the droplet Reynolds number is given by

$$Re_d = \frac{D_d \rho_g |V_g - V_d|}{\mu_m} \quad , \qquad (20)$$

and the modified viscosity is

$$\mu_m = \frac{\mu_g}{(1 - \alpha_d)^{2.5}} \quad . \qquad (21)$$

By increasing the gas viscosity this correlation takes into account the increased drag on the non-spherical shape of the droplets.[3] Also, by using a modified viscosity, the droplet-to-droplet interactions and the existence of a multitude of droplets in the channel are accounted for.

The combination of Eqs. (18)–(21) provides a method for calculating the droplet velocity. However, because the drag coefficient is dependent on the Reynolds number, which in turn is dependent on the droplet velocity, the equations must be solved by iteration. To avoid performing the iterative solution, one can make a rough estimate of the droplet velocity by assuming a spherical droplet that is unaffected by the presence of the surrounding droplets. Bird, Stewart, and Lightfoot[15] recommend a constant drag coefficient of 0.44. In this case, the droplet velocity becomes

$$V_d = V_g - 2.462 \left(\frac{\Delta\rho}{\rho_g} g_c \frac{D_d}{2}\right)^{1/2} \quad . \qquad (22)$$

To determine the relative accuracy of the above equation to the more detailed model, a computer program was written to solve Eqs. (18) (21) by iteration and compare them to the droplet velocity given by Eq. (22). For a given area fraction of droplet and gas velocity, the droplet diameter is first calculated with Eq. (16). Then, Eqs. (18) (21) are solved by iteration for the droplet velocity using bisection. This is carried out for a variety of vapor velocities. The results for a void fraction of 0.95 with air-water and gas velocities ranging from 20 to 60 m/s are given in Fig. 2. The droplet velocity using the more detailed model [Eqs. (18) (21)] is slightly lower than the spherical droplet model [Eq. (22)] at the low gas velocities. This is consistent with the drag coefficient, which is lower than 0.44. At about 28 m/s, the two models give the same drag coefficient and therefore predict the same droplet velocity. At the higher gas flows, the detailed model gives a higher drag coefficient and therefore predicts a higher droplet velocity. The sensitivity of the droplet velocity to the drag coefficient is relatively small because the droplet velocity is proportional to the inverse of the square root of the drag coefficient [Eq. (18)]. Calculations at other void fractions show similar results, and in general the simplified approach gives results within 2.5% of the detailed approach. The numerical iteration was

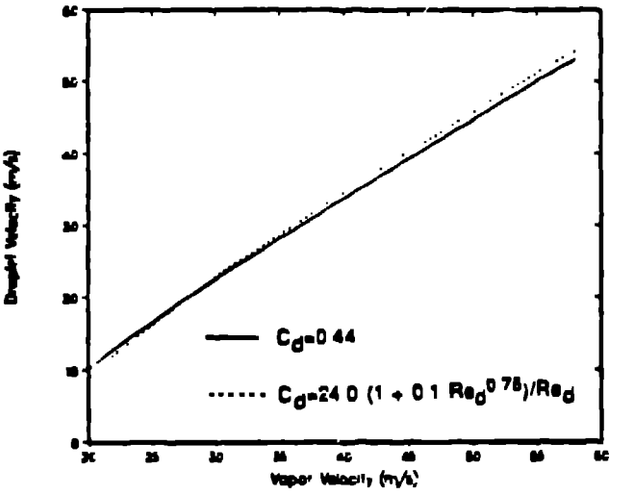

Fig. 2. Droplet velocity comparison.

performed to an accuracy (difference in solution value between successive iterations) of less than 0.1%.

Film Velocity

The film velocity can be estimated using the continuity equation for the liquid and the definition of entrainment. The flow of liquid is equal to the flow of droplets plus the flow of the film. This can be written in terms of the superficial velocities because the density of the droplets and film are the same. Combining the definition of entrainment [Eq. (3)] with the definition of the superficial film velocity [Eq. (2)] and solving for the liquid film velocity, we have

$$V_f = \frac{j_l}{\alpha_l}(1 - E) \quad . \tag{23}$$

This relationship is somewhat disturbing in the fact that as the entrainment fraction approaches 1.0, the liquid film velocity approaches 0.0 even though there may still exist a substantial amount of liquid film (Eq. 3). A simple fix to this problem is to correlate the entrainment data with a new definition for entrainment, that is the area fraction of droplets divided by the area fraction of liquid.

Following the development given by Ishii and Chawla,[3] the drag force on the droplets balances with the total pressure drop. From the definition of the droplet form drag and the droplet momentum equation the interfacial droplet drag coefficient is

$$C_{id} = \frac{\frac{3}{4}\alpha_d \rho_g C_d}{D_d} \quad . \tag{24}$$

To determine the interfacial drag coefficient, estimates are required for the drop diameter, the area fraction of droplets, and the droplet drag coefficient. The droplet diameter is given by Eq. (16), the droplet drag coefficient by Eq. (19), the area fraction of droplets from the definition of entrainment by Eq. (3), and an entrainment correlation by Eq. (13). The droplet velocity can be obtained using the iterative solution to Eqs. (18)–(21) or with Eq. (22) directly.

To determine the interfacial drag coefficient, Ci_f, required for the film momentum equation, we integrate the shear stress at the gas core to film interface over a given length, thus providing the contribution of the interfacial drag on the film as a function of the pressure drop.

Using the definition for the film shear stress, and the diameter of the core region, the interfacial drag between the film and gas core is given by

$$Ci_f = \frac{2 f_i \rho_c (\alpha_g + \alpha_d)^{1/2}}{D} \quad . \tag{25}$$

where the core density is typically approximated by using the density of the gas. However, for the modified Wallis correlation (see below), a density estimate is made that includes the effect of droplets flowing with the gas:

$$\rho_c = \frac{\alpha_g V_g \rho_g + \alpha_d V_d \rho_l}{\alpha_g V_g + \alpha_d V_d} \quad . \tag{26}$$

Because the liquid density is typically 200–500 times the gas density, a small increase in the droplet fraction can have a significant effect on the core density. This method of estimating the core density is also recommended by Hewitt.[16]

To solve for Ci_f, the interfacial friction f_i is required. Several correlations for this term exist in the literature. For this study, four correlations are tested: Wallis, modified Wallis, Henstock and Hanratty, and Barathan.

Wallis[4] proposed two correlations for the interfacial friction: a simple correlation with constant coefficients and a more detailed correlation. For the purpose of comparison, we refer to these as the Wallis and modified Wallis correlations, respectively.

The Wallis correlation is given by

$$f_i = 0.005(1 + 75\,\alpha_f) \quad . \tag{27}$$

This correlation is analogous to the wall shear equation for a pipe, including the effect of roughness. The constant 0.005 represents the smooth tube friction. It is theorized that as the liquid film fraction increases, waves build up and effectively increase the roughness of the interface, thereby increasing the interfacial friction.

As an improvement, Wallis offered a modified version of this simple correlation to account for the increased density of the gas core, variable smooth tube friction, and the upward movement of the liquid gas core interface (which reduces the relative velocity between the core and film):

$$\tau_i = 2 f_i \rho_c (V_g - 2V_f)^2 \quad , \tag{28}$$

$$f_i = 0.079\, Re_c^{-0.25}(1 + 75\,\alpha_f) \quad , \text{ and} \tag{29}$$

$$Re_c = \frac{D(\rho_g V_g \alpha_g + \rho_l V_d \alpha_d)}{\mu_g} \quad . \qquad (30)$$

Barathan[8] developed a correlation for countercurrent, annular-mist flow. In this case, the vapor velocity was sufficiently low that the film flowed downward. Although this situation is different than the co-current problem being considered, it is advantageous to test this correlation because the mechanisms are similar and the effect of pipe diameter is included. The correlation is given as

$$f_i = 0.005 + A\,\delta^{*B} \quad , \qquad (31)$$

where A, δ^* and B are functions of the fluid conditions, velocity and the pipe diameter. Because the correlation is developed for countercurrent flow, a relatively high interfacial friction is expected.

Henstock and Hanratty propose the following interfacial friction correlation for co-current flow:

$$f_i = f_s(1 + 1400\,F) \quad , \qquad (32)$$

where f_s and F are functions of the fluid properties and the gas and liquid velocities.

To determine the wall drag contribution, we define a relationship for C_{wk}, where k refers to either the gas or the liquid film. These terms are multiplied by their respective V^2s in the two-fluid momentum equation. A relation for C_{wk} can be developed in the same manner as the film interfacial drag coefficient. Performing a momentum balance at the wall we find

$$C_{wk} = \frac{2 f_{wk} \rho_k}{D} \quad . \qquad (33)$$

The wall friction factor is given by

$$f_{wk} = \frac{16}{Re_k} \qquad (34)$$

for laminar flow and

$$f_{wk} = 0.046\,Re_k^{-0.2} \qquad (35)$$

for turbulent flow.

In the case of annular flow, the gas is never in contact with the wall, and therefore the gas wall drag term can be eliminated. However, Lin[7] has shown that a minimum film thickness exists at which point rivulets form. In this case, the gas can come in contact with the wall and add to the wall drag term. To take this effect into account, an ad hoc weighting factor is developed that is applied to the respective wall drag terms.

gas phase: $C_{wg} = \frac{2 f_{wg} \rho_g}{D}(1 - WFRIV)$, and (36)

liquid phase: $C_{wl} = \frac{2 f_{wl} \rho_l}{D}(WFRIV)$, (37)

$$WFRIV = \frac{\alpha_f}{\max(\alpha_f, \frac{f_{lmin}}{D})} \quad . \qquad (38)$$

The value of f_{lmin} is the minimum film thickness and is taken to be 0.0001 m, based on engineering judgment. The use of the ratio $\frac{f_{lmin}}{D}$ in the denominator of the equation above is consistent because for thin films, the liquid film fraction can be approximated by the film thickness divided by the diameter. As the film fraction decreases below the minimum film thickness, the use of WFRIV allows the wall drag from the gas to phase in and the wall drag from the liquid to be phased out in a continuous manner.

For given superficial gas and liquid velocities, it is desired to calculate the total liquid fraction using the two-fluid momentum equations so that comparisons can be made to the data. A control volume approach is used, eliminating the need for spatial discrimination. By combining the liquid and gas momentum equations [Eqs. (7) and (8)], the following balance equation results:

$$0 = C_i V_r^2 - \alpha_g C_{wl} V_l^2 + \alpha_l C_{wg} V_g^2 - \alpha_g \alpha_l \Delta\rho g_c \quad . \qquad (39)$$

Because the coefficients are dependent on the various area fractions and field velocities, the above equation is transcendental and requires an iterative solution for the liquid fraction. A utility program has been developed to solve the equations and assess the various film drag models. For the data comparison the total liquid fraction, α_l, was solved for by iteration to an accuracy of 0.1%.

The data of Hossfeld and Barathan were chosen for the assessment calculations because pipe diameters of 0.051 m and 0.152 m were both tested. The experimental setup consists of a vertical test section, with inlet and outlet plenums attached. Air and water are forced into the bottom of the test section and allowed to flow vertically upwards. The data are presented for the total liquid fraction (representing both the droplet and film components) in terms of the dimensionless gas and liquid velocities. These are defined as

$$j_g^* = j_g\left(\frac{\rho_g}{g_c D \Delta\rho}\right)^{1/2} \quad , \text{ and} \qquad (40)$$

$$j_l^* = j_l\left(\frac{\rho_l}{g_c D \Delta\rho}\right)^{1/2} \quad . \qquad (41)$$

For a particular liquid injection rate (dimensionless liquid velocity), several gas flows were tested. For each set of conditions, the liquid fraction was measured after the flows had reached steady state.

RESULTS

For the initial comparisons, a single data set was used: 0.152-m diam and j_f-star (dimensionless superficial liquid injection rate) of 0.067. The results are plotted as the liquid fraction vs the dimensionless superficial gas velocity (j_g-star). As expected the data shows that as the gas flux increases the total liquid fraction decreases as the film thickness decreases. Although the droplet entrainment increases, the total liquid fraction is dominated by the film component and therefore decreases with the higher gas flux. The result using the Wallis correlation is given in Fig. 3. The data comparison for the modified Wallis correlation, the Henstock and Hanratty correlation, the Barathan correlation, and the EPRI drift-flux model are shown in Figs. 4–7,

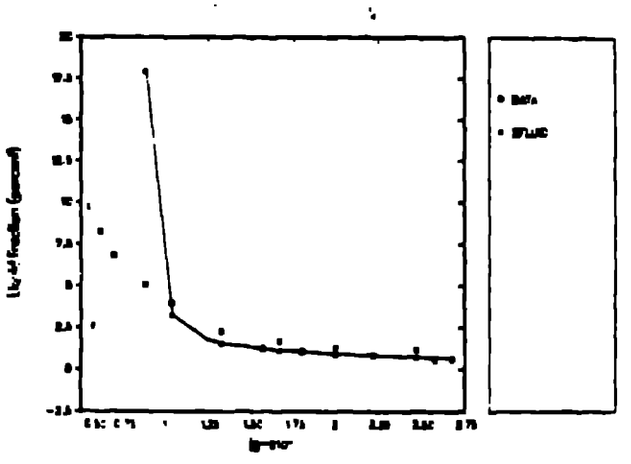

Fig. 3. Liquid fraction comparison. two-fluid solution using the Wallis correlation and limiting the entrainment to 0.8.

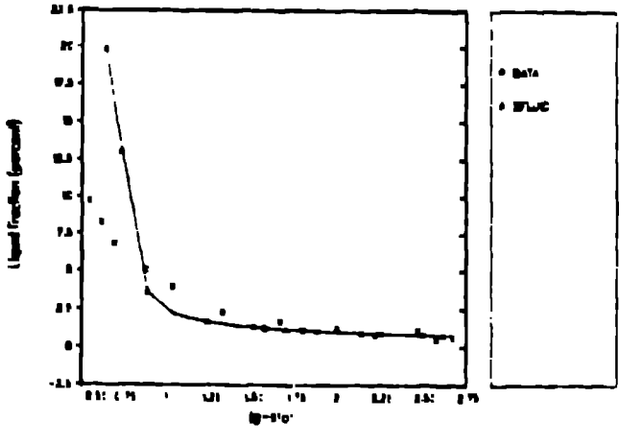

Fig. 4. Liquid fraction comparison using the modified Wallis correlation.

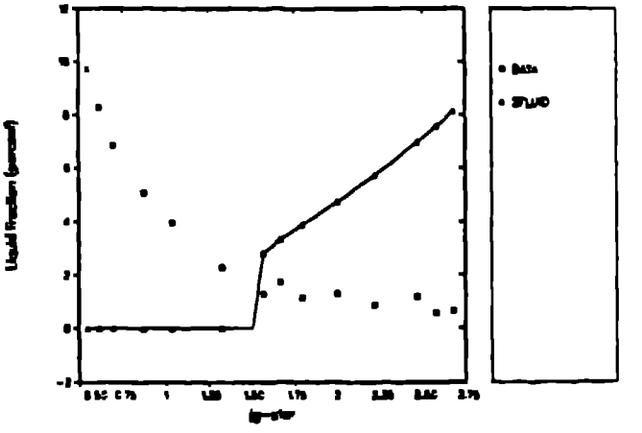

Fig. 5. Liquid fraction comparison using the Henstock and Hanratty correlation.

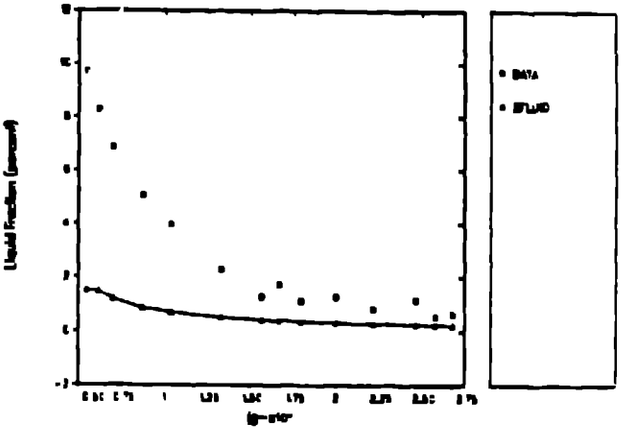

Fig. 6. Liquid fraction comparison using the Barathan correlation.

respectively. In all the figures, the data are shown as unconnected circles.

As noted in the figure captions, we have limited the entrainment fraction to a value of 0.8. This was the value observed in the data although the authors have prescribed no quantitative accuracy to it. Restricting the entrainment fraction was necessary to avoid the inconsistency that was noted above. That is, as the entrainment fraction approaches 1.0 the film velocity approaches 0.0 (Eq. 23), but there may still be a substantial amount of liquid film (Eq. 3). The entrainment correlation that we use (Eq. 13) appears to be difficient for this case as it predicts an entrainment fraction of 1.0 for moderate gas flux whereas the data suggest a maximum entrainment of 0.8. Thus, the entrainment was restricted to this value.

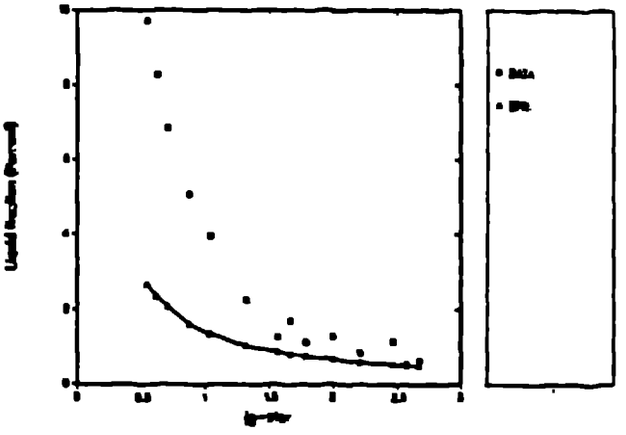

Fig. 7. Liquid fraction comparison using the EPRI drift-flux model.

The Wallis correlation comparison (Fig. 3) showed good agreement in the mid- and high-range of the gas velocities but poor comparisons at the low values. Use of the modified Wallis correlation (Fig. 4) shows a slight improvement at the low range of gas velocities and maintains the excellent comparisons in the mid- and high-range of gas velocities.

The Henstock and Hanratty correlation (Fig. 5) produces an incorrect trend when compared with the data. The functional form of the correlation shows that as the gas velocity increases, the overall film interfacial friction factor decreases. This causes an increase in the liquid fraction with increasing gas velocity. As demonstrated in the comparison, the data show the opposite trend.

The Barathan correlation (Fig. 6) underpredicts the data over the entire range. This result was expected because this correlation was developed for conditions of countercurrent flow, rather than co-current as is assumed here. Thus, the predicted interfacial friction is too high, which in turn causes less accumulation of liquid.

The EPRI model (Fig. 7) is shown to underpredict the data through most of the range of gas velocities. Although the correlation is quantitatively deficient, the correct trend is predicted.

From these initial comparisons, it appears that the modified Wallis correlation provides the overall best prediction of the data. An assessment is made with the modified Wallis correlation against the other data provided by Hossfeld and Barathan. Comparisons with the small-diameter data show a good prediction at the low liquid injection rate, but an underprediction of the liquid fraction data at the high liquid injection rates.

Solving for C_1 in Eq. 39 (given the liquid fraction, gas, and liquid fluxes as input), we can calculate the required film friction factor using the data values for the liquid fraction and gas and liquid fluxes. No iteration is required. A program was written to do this with the five data sets previously chosen (three sets for the 0.051-m-diam and two sets for the 0.152-m-diam pipes). We assumed that the mixture properties are used for the gas core as is used in the modified Wallis correlation. The trend in the data shows an increasing friction factor as the liquid fraction is increased. Also, the data seem to indicate that the friction factor is relatively independent of pipe diameter. Using a least squares fit and the independent variable as the liquid film fraction a resulting correlation for the film friction factor is developed

$$f_i = 0.0033 + 0.0144\,\alpha_f + 2.0404\,\alpha_f^2 . \quad (42)$$

Using this new correlation and the assumption that the interface travels at the speed of the mass average velocity, the prediction of the liquid fraction data is improved. The comparisons for the two large-diameter cases and the small-diameter cases are shown in Figs. 8–12. The new correlation is shown to provide a better prediction of the data for all the data sets, especially for the small diameter. However, it is recognized that this correlation was developed with a very limited set of data and is restricted in its application. The author needs to correlate a wider range of data (down flow, steam water, etc.) in the future using a similar procedure before it is acceptable for use in a large systems code such as TRAC.

In conclusion the results show that when used with the two-fluid model, the modified Wallis correlation performs the best overall in predicting the liquid fraction data assuming that we restrict the entrainment fraction to what was observed. The Henstock and Hanratty correlation is shown to predict the incorrect trend, and both the Barathan correlation and the EPRI drift-flux model underpredict the data. A new correlation was developed for the interfacial film friction that in conjunction with the other model assumptions provides good agreement for both large and small pipe data. At large liquid injection rates, however, the prediction is still deficient. Future work is recommended to perform a detailed investigation of the core-to-film interface in the hope of developing a better interfacial film friction correlation that can better predict the data over a wide range of

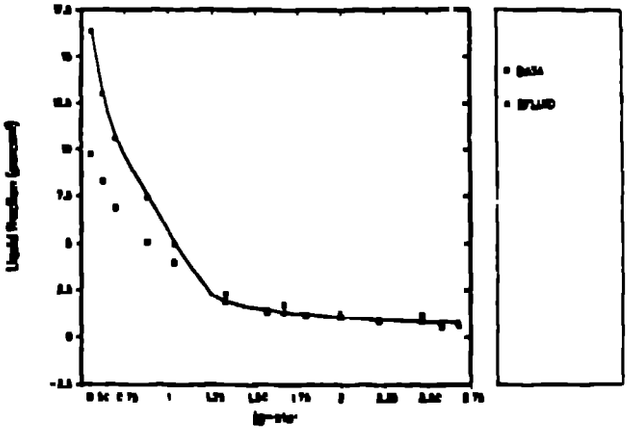

Fig. 8. Liquid fraction comparison using the new correlation: 0.152-m diam and a dimensionless liquid injection rate of 0.067.

diameters. Future work should also extend the development to downflow, steam water flow and other geometry if possible. Based on this work it is therefore recommended that the modified Wallis correlation be used in two-fluid system analysis codes such as TRAC.

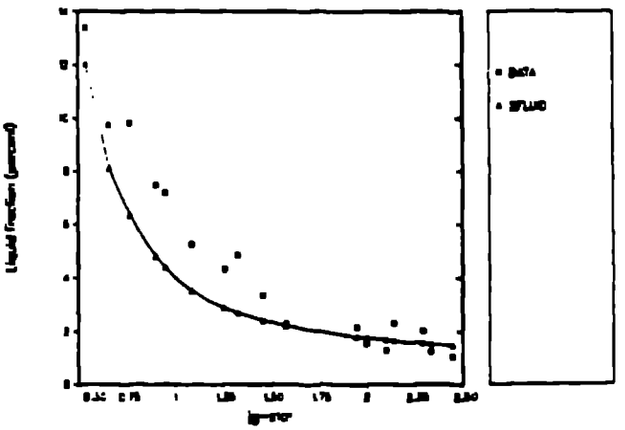

Fig. 9. Liquid fraction comparison using the new correlation: 0.152-m diam and a dimensionless liquid injection rate of 0.134.

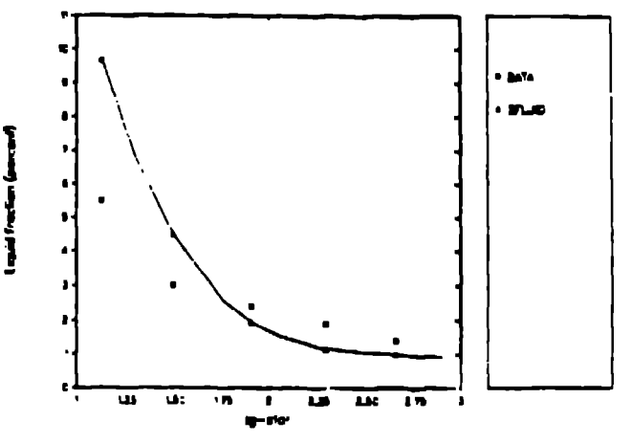

Fig. 10. Liquid fraction comparison using the new correlation: 0.051-m diam and a dimensionless liquid injection rate of 0.076.

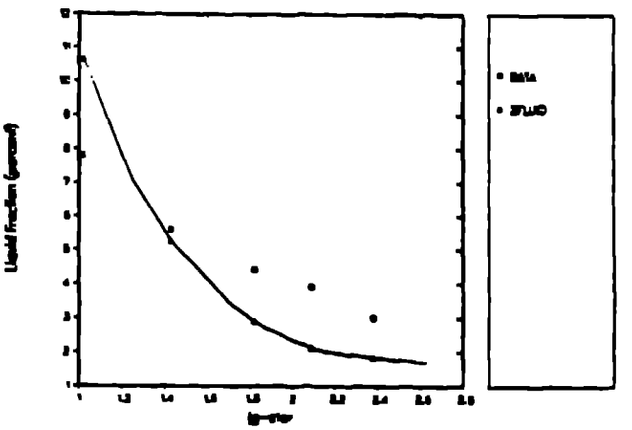

Fig. 11. Liquid fraction comparison using the new correlation: 0.051-m diam and a dimensionless liquid injection rate of 0.153.

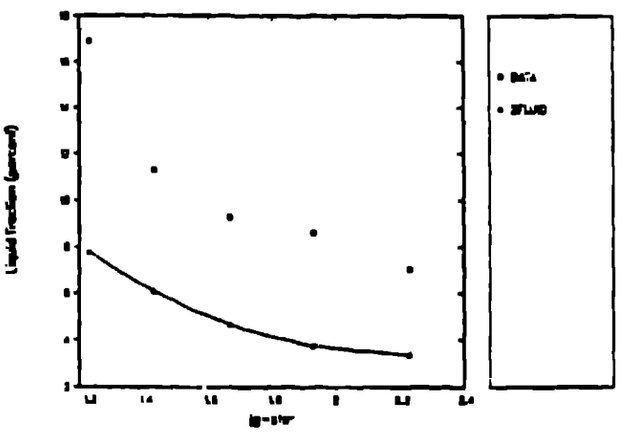

Fig. 12. Liquid fraction comparison using the new correlation: 0.051-m diam and a dimensionless liquid injection rate of 0.394.

REFERENCES

1. D. R.LILES and J. H. MAHAFFY, et al., "TRAC-PF1/MOD1: An Advanced Best-Estimate Computer Program for Pressurized Water Reactor Thermal-Hydraulic Analysis," Nuclear Regulatory Commission report NUREG/CR-3858, Los Alamos National Laboratory report LA-10157-MS (July 1986).

2. V. H. RANSOM, et al., "RELAP5/MOD2 Code Manual Volume 1, System Models and Numerical Methods," EG&G Idaho Inc. (1982).

3. M. ISHII and T. C. CHAWLA, "Local Drag Laws in Dispersed Two-Phase Flow," Nuclar Regulatory Commission report NUREG/CR=1230 (December 1979).

4. G. B. WALLIS, *One Dimensional Two Phase Flow* (McGraw-Hill, 1969).

5. I. KATAOKA and M. ISHII, "Mechanism and Correlation of Droplet Entrainment and Deposition in Annular Two-Phase Flow," Nuclear Regulatory Commission report NUP /CR-2885 (July 1982).

6. S. M. SAMI, "An Improved Numerical Model for Annular Two-Phase Flow with Liquid Entrainment," Int. Comm. Heat Mass Transfer, Vol. 15, pp. 281-292 (1988).

7. N. K. POPOV and U. S. ROHATGI, "Analysis of Counter-Current Adiabatic Flow Limitation Phenomenon in Vertical Pipes," Nuclear Regulatory Commission report NUREG/CR-4630 (September 1986).

8. D. BARATHAN, G. B. WALLIS, and H. J. RICHTER, "Air-Water Counter- current Annular Flow," Electrical Power Research Institute report EPRI NP-1165, RP-443-2 (1979).

9. W. H. HENSTOCK and T. J. HANRATTY, "The interfacial Drag and the Height of the Wall Layer in Annular Flows," AIChE Journal, Vol. 22, No. 6, p. 990 (1976).

10. M. ISHII and K. MISHIMA, "Two-Fluid Model and Hydrodynamic Constitutive Relations," Nuclear Engineering and Design, Vol. 82, pp. 107-126 (1984).

11. L. M. HOSSFELD and D. BARATHAN, "Interfacial Friction in Co-current Upward Annular Flow," Electrical Research Institute report EPRI NP-2326, Research Project 443-2 (March 1982).

12. I. KATAOKA, M. ISHII, and K. MISHIMA, "Generation and Size Distribution of Droplet in Annular Two-Phase Flow," Transactions of the ASME, Vol. 105, pp. 230-238 (June 1983).

13. B. CHEXAL and G. LELLOUCHE, "A Full-Range Drift Flux Correlation for Vertical Flows (Revision 1)," Electric Power Research Institute report NP-3989-SR, Revision 1 (September 1986).

14. B. CHEXAL, J. HOROWITZ, and G. LELLOUCHE, "An Assessment of Eight Void Fraction Models for Vertical Flows," Nuclear Safety Analysis Center report NSAC-107, EPRI (December 1986).

15. R. B. BIRD, W. STEWART, and E. LIGHTFOOT, *Transport Phenomena* (John Wiley and Sons 1960).

16. A. BERGLES, J. COLLIER, J. DELHAYE, G HEWITT, and F. MAYINGER, *Two-Phase Flow and Heat Transfer in the Power and Process Industries* (Hemisphere Publishing Co., 1981).

17. P. Y. LIN and T. J. HANRATTY, "Effect of Pipe Diameter on Flow Patterns for Air-Water Flow in Horizontal Pipes," Int. J. Multiphase Flow Vol. 13, No. 4, pp. 549-563 (1987).